Metal–Graphene Catalysis

Deutsche Ausgabe: DOI: 10.1002/ange.201508908
Internationale Ausgabe: DOI: 10.1002/anie.201508908

One-Step Pyrolysis Preparation of 1.1.1 Oriented Gold Nanoplatelets Supported on Graphene and Six Orders of Magnitude Enhancement of the Resulting Catalytic Activity

Ana Primo, Ivan Esteve-Adell, Simona N. Coman, Natalia Candu, Vasile I. Parvulescu, and Hermenegildo Garcia**

Abstract: *Pyrolysis of chitosan films containing Au^{3+} renders 1.1.1 oriented Au nanoplatelets (20 nm lateral size, 3–4 nm height) on a few layers of N-doped graphene ($\overline{Au}$/fl-G), while the lateral sides were 0.0.1 oriented. Comparison of the catalytic activity of $\overline{Au}$/fl-G films with powders of unoriented Au NPs supported on graphene showed that $\overline{Au}$/fl-G films exhibit six orders of magnitude enhancement for three gold-catalyzed reactions, namely, Ullmann-like homocoupling, C–N cross coupling, and the oxidative coupling of benzene to benzoic acid. This enhancement is the result of the defined morphology, facet orientation of Au nanocrystals, and strong gold-graphene interaction.*

Catalysis by supported metal nanoparticles (MNPs) has been a very active field of research in the last thirty years.[1] Remarkable examples of highly active and selective MNP catalysts for organic transformations include aerobic oxidations, couplings, and rearrangements.[1] Catalysis by gold constitutes one of the most salient examples of unforeseen properties for a material that appear exclusively at the nanoscale.[2–4] A constant target in this area has been the development of more efficient Au catalysts, and this has been generally achieved by changing the support and average particle size. However, according to an existing theory,[5,6] control of the crystallographic facet exposed by the NP should be a powerful tool to boost catalytic activity. Experimental support of this concept has remained elusive owing to the difficulty in preparing MNPs having preferential facet orientation, and there are only a few examples of highly active, morphologically defined Au nanocrystals.[6–9] There has been, therefore, an interest in developing synthetic strategies for the preparation of oriented Au NPs, although the success has been limited until recently.[10–13] The preparation of colloidal solutions of Au nanocrystals with defined morphologies and exposed facets was recently achieved by using additives that coordinate strongly to one facet, arresting its growth in comparison to other crystallographic planes.[14,15] These oriented Au nanocrystals can be subsequently supported on a solid, aimed at adsorption of the nanocrystal with some preferential orientation. Graphenes are among the currently preferred supports, owing to their large surface area, easy dispersability, and strong metal–support interactions. There are now numerous examples showing that the catalytic activity of MNPs supported on graphene is higher than the activity of analogous MNPs supported on other carbon forms or metal oxides.[16–18]

Herein, we report the preparation of 1.1.1 facet-oriented Au nanoplatelets of average lateral dimension 20 nm and 3–4 nm height, supported on a few layers of N-doped graphene films ($\overline{Au}$/fl-G, $\overline{Au}$: 1.1.1 oriented Au nanoplatelets, fl: few layers, G: graphene) that exhibit about six orders of magnitude higher catalytic activity than the analogous unoriented Au catalyst (Au/fl-G) for three different gold-catalyzed reactions.

The preparation of $\overline{Au}$/fl-G is based on the formation of N-doped G by simultaneous pyrolysis of nanometric films on quartz under inert atmosphere at 900 °C of a natural biopolymer (chitosan), and Au nanoplatelets by reduction of Au(III). The Au particles are morphologically nanoplatelets, and their dimensions range from 20 nm to larger than 1000 nm, depending on the Au loading on the polymeric precursor. In a related system, it was reported that Cu_2O nanocrystals supported on G exhibit greatly enhanced catalytic activity.[19]

Pyrolysis is known to convert chitosan and other filmogenic natural polysaccharides into G.[20] Apparently, the fibrils of chitosan, the carbonaceous residues derived from them, and the evolving N-doped G arrest in each step the growth of Au NPs forming simultaneously in the process, as a consequence of the reductive conditions of the G synthesis and the low solubility of Au on carbon.[21,22] While many metals form metal carbides upon heating the metal with carbon at high temperatures, the noble character of Au results in a phase segregation, leading to the synchronous formation of N-doped G and Au NPs. Remarkably, despite the high pyrolysis temperature, the average lateral size of the Au nanoplatelets can be as small as 20 nm for films with low Au loading (ng cm^{-2}). Besides being a precursor of N-doped G, one of the key points in the synthesis is the ability of chitosan films to adsorb metal ions by strong interactions with the positive

[*] Dr. A. Primo, I. Esteve-Adell, Prof. H. Garcia
Instituto Universitario de Tecnología Química CSIC-UPV
Universidad Politécnica de Valencia
Avda. de los Naranjos s/n, 46022 Valencia (Spain)
E-mail: hgarcia@qim.upv.es
Dr. S. N. Coman, N. Candu, Prof. V. I. Parvulescu
Department of Organic Chemistry, Biochemistry, and Catalysis
University of Bucharest
Bd. Regina Elisabeta nr. 4–12, 030018 Bucharest (Romania)
E-mail: vasile.parvulescu@chimie.unibuc.ro

Supporting information and ORCID(s) from the author(s) for this article are available on the WWW under http://dx.doi.org/10.1002/anie.201508908.

amino groups of the glucosamine units of the polymer fibrils and metal anions, in this case $AuCl_4^-$.

The loading of Au NPs on the G film can be controlled by varying the concentration of $AuCl_4^-$ in the solution during impregnation of chitosan films (Scheme 1). In this way, Au

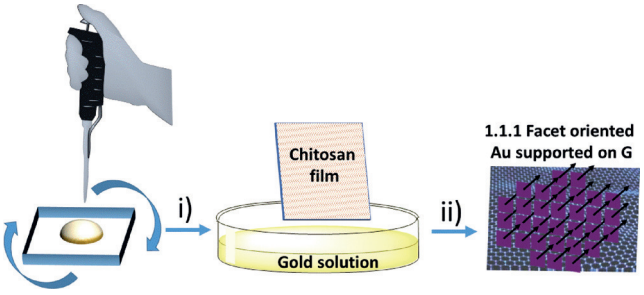

Scheme 1. Preparation procedure for Au/fl-G films. (i) Spin coating of an aqueous chitosan solution on quartz ($2\times2\ cm^2$); (ii) Adsorption of $AuCl_4^-$ on chitosan film before pyrolysis under inert atmosphere at 900 °C.

loadings from a few $ng\,cm^{-2}$ up to $\mu g\,cm^{-2}$ on the Au/fl-G film can be obtained in a reproducible way. The preparation procedure was repeated independently many times with identical Au nanocrystal orientation and consistent characterization data for the Au/fl-G films. This one-step synthesis of Au/fl-G contrasts with other reported methods for the preparation of Au NPs supported on G that require prior preparation of G,[23] and even modification of the G surface.[24]

For the sake of comparison, Au/fl-G powders were also synthesized by supporting preformed Au NPs on N-doped G (see the Experimental Section).

XRD of Au/fl-G samples (loading of Au 3.2 $ng\,cm^{-2}$) did not exhibit any peaks, owing to the low film thickness and Au loading. In contrast, thicker samples of multilayer G (ml-G, ml: multilayer; thickness > 40 nm) containing Au exhibit a single peak at 39°, accompanied by a weaker 2.2.2 peak at 82°, characteristic of 1.1.1 oriented crystals. Figure 1 shows

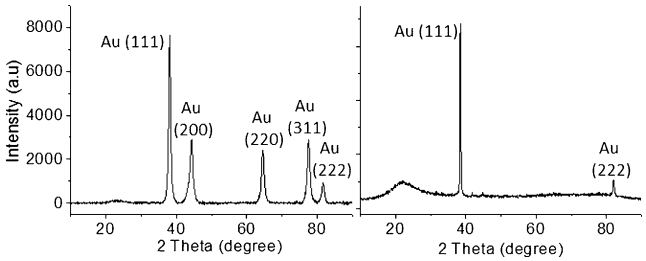

Figure 1. XRD patterns of Au/fl-G (1 wt%; left) and Au/mL-G ($2.4\ \mu g\times cm^{-2}$; right) showing the different indexation of the peaks. The broad band at about 22° observed in the Au/mL-G corresponds to the characteristic diffraction of ml-G.

XRD of Au/mL-G (Au loading $2.4\ \mu g\times cm^{-2}$) compared to Au/fl-G (Au loading 1 wt%) lacking any preferential orientation. In the latter case, XRD presents more diffraction peaks that correspond indisputably to c Au crystals (JCPDS No 01-1174). As seen in Figure 1, the consequence of the simultaneous formation of N-doped G and Au NPs is the orientation of the Au NPs crystals.

Possible explanations to rationalize the preferential growth of the 1.1.1 facets include the combination of higher thermodynamic stability of this facet, together with a templation effect of N-doped G on the growth of Au nanoplatelets. This explanation is based on the accepted mechanism for the chemical vapor deposition of G on metal surfaces.[21,25,26] In these syntheses of G, it is accepted that carbon atoms start to deposit on the metal surface and the metal atoms template the hexagonal arrangement of the growing G formed epitaxially on the metal surface. In our system, the process would be reversed: as G sheets are formed in the pyrolysis from chitosan, Au atoms evolving from the polymeric fibrils will appear on the surface of G, resulting in an epitaxial growth of the 1.1.1 facets of Au nanoplatelets deposited on G, thereby maximizing the interaction between the Au atoms and G (Supplementary Information, Figure S1).

Direct information on the morphology of Au crystals and their preferential 1.1.1 facet orientation, regardless of the loading of Au and thickness of G, was obtained by electron microscopy. TEM images of Au/G (both fl and ml) samples revealed that the preferential morphology of Au nanocrystals is nanoplatelets, whose size distribution and average dimensions depend on the concentration of Au on chitosan. Low-loading Au/fl-G films have a Au content of $3.2\ ng\,cm^{-2}$ ($16.2\ pmol\,cm^{-2}$). For low-loading Au/fl-G films that do not exhibit any XRD pattern, the average lateral dimension of the nanoplatelets determined by TEM was about 20 nm (Figure 2; Supporting Information, Figures S2 and S3). A few nanoplatelets detached from the G surface, allowing estimation of a 3–4 nm for the thickness of these nanoplatelets (see marked nanoplatelets in Figure S4), an estimation that was confirmed more accurately by AFM. It is worth noting that these relatively small average dimensions are remarkable considering the high temperature required in the synthesis of Au/fl-G films and the known tendency of Au NPs to undergo aggregation at high temperatures. For these films with low Au loading, as well as for those with larger Au loading, transmission Kikuchi diffraction[27] of relatively large film areas ($2.5\times2.5\ \mu m^2$) showed the preferential 1.1.1 facet orientation of Au nanoplatelets (Figure 2; Supporting Information, Figure S5), consistent with the XRD of the thicker Au/mL-G films. Comparison of the FESEM images showing the presence of Au with that of the 1.1.1 facet based on the transmission electron diffraction pattern showed a coincidence over 90%. Moreover, these images also reveal the strict 0.0.1 orientation of the planes perpendicular to the larger 1.1.1 surface. Another interesting observation related to the interplay between Au and G is the presence on G of some pathways around Au nanoplatelets with significantly decreased thickness of the G sheet. It seems that formation of Au nanoplatelets causes depletion on the number of G layers, possibly owing to the activity of Au nanoplatelets as catalytic sites improving graphitization by removal of residual oxygenated functional groups or the random walk of Au nanocrystals on the G sheets defining some pathways. AFM

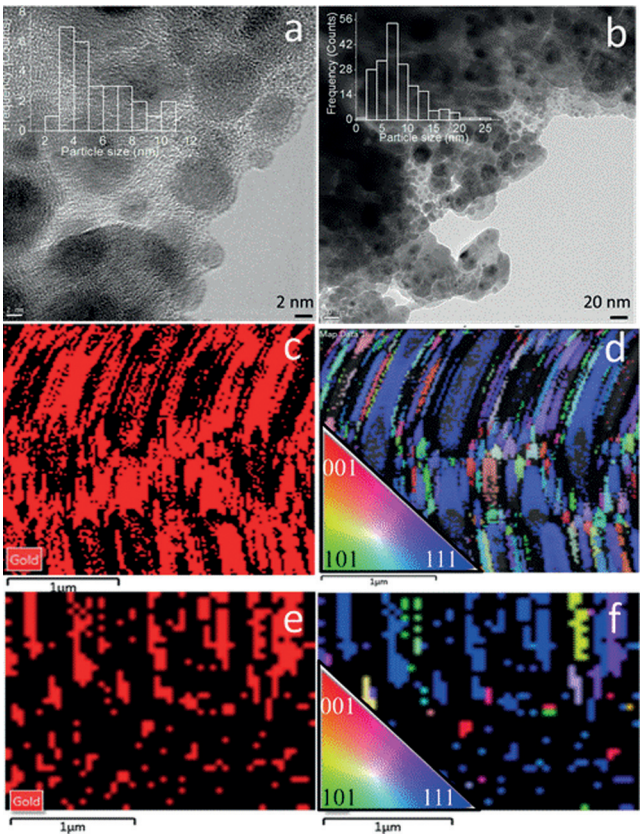

Figure 2. a and b) TEM images of $\overline{\text{Au}}$/fl-G (3.2 ng cm^{-2}) at two different magnifications. Insets: corresponding particle size distribution. c and e) EDS analysis of Au of two different films (Au loading = 3.2 ng × cm^{-2}) showing the presence of Au in red. d and f) Facet orientation of the nanoplatelets presented the 1.1.1 facet (blue) and the 0.0.1 planes (pink) obtained by transmission Kikuchi diffraction.[27] Insets: color codes.

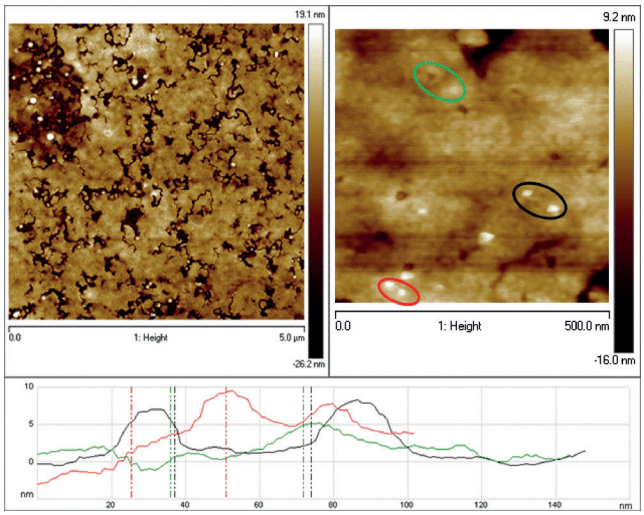

Figure 3. Top view at two different magnifications of the AFM image taken for $\overline{\text{Au}}$/fl-G (3.2 ng cm^{-2}). The size (height and lateral dimensions) of five Au nanoplatelets circled in the right frame are presented in the bottom part of the image. Notice that according to the low magnification image shown in the left frame, Au nanoplatelets are consistently located on valleys of the G film of height lower than 10 nm.

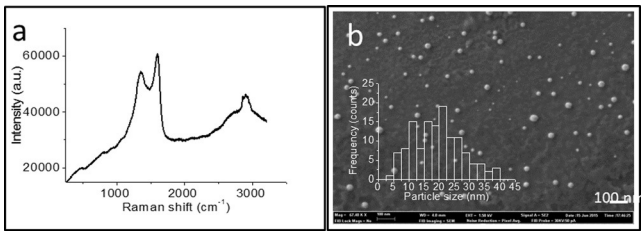

Figure 4. a) Raman spectrum of $\overline{\text{Au}}$/fl-G (3.2 ng cm^{-2}). The presence of a sharp 2D band on top of a broad 2D background can be clearly observed at 2850 cm^{-1}. b) SEM image of $\overline{\text{Au}}$/fl-G (3.2 ng cm^{-2}). Inset: particle size distribution.

measurements of $\overline{\text{Au}}$/fl-G also confirm the nanoplatelet morphology of Au crystals and their uniform height of about 3–4 nm. Figure 3 and Figure S6 (Supporting Information) show top views of $\overline{\text{Au}}$/fl-G, as well as measurements of the height of Au nanoplatelets distributed on a relatively large area of the $\overline{\text{Au}}$/fl-G film. Cuts on the film indicate that the thickness of the G is about 20 nm, although there are certain areas around Au crystals with G thickness about 8 nm. The existence of certain pathways around Au nanoplatelets observed in FESEM is also seen in the top AFM images of $\overline{\text{Au}}$/fl-G, which show that most Au nanoplatelets are located in valleys of the G film.

The Raman spectrum of $\overline{\text{Au}}$/fl-G (Figure 4) shows the characteristic G and D bands appearing at 1600 and 1350 cm^{-1}, accompanied by a broad 2D band around 2700 cm^{-1}, expected for G obtained by pyrolysis of chitosan. The I_G/I_D ratio was 1.13, which is a common value for this G with N-doping (from glucosamine units of chitosan) and residual O functionalities.[28] An abnormal feature of the Raman spectrum was, however, the appearance of a sharp peak at about 2850 cm^{-1} on top of the broad 2D band. The appearance of a narrow 2D peak is generally associated to the presence of single or double G layers. It is likely that this sharp 2D, not observed in analogous G samples, arises as consequence of the influence of Au nanoplatelets on G, making the G film in the surroundings of the Au nanoplatelets thinner and increasing the intensity of the band by plasmon Raman enhancement. It is noteworthy that the position of the 2D band appears generally at values below 2750 cm^{-1}.[24] Other groups have observed this shift and attributed it to charge transfer from G to the adsorbate.[29] Accordingly, the abnormal shift of the 2D band toward higher values could be attributed to a charge transfer from G to Au nanoplatelets, owing to the different work function of the two components.

X-ray photoelectron spectroscopy (XPS) established the composition and distribution of each element in the material into different coordination environments. As expected, the $\overline{\text{Au}}$/fl-G films contain C (89 at %), N (1 at %), O (5 at %), and Au (4 at %). Figure 5 and Figure S7 (Supporting Information) also show the high-resolution C 1s and the Au 4f peaks recorded for $\overline{\text{Au}}$/fl-G. The experimental C 1s peak can be deconvoluted into three main contributions of 66, 28, and 6 %, corresponding to graphenic sp2 (284.5 eV), C=O/C–N

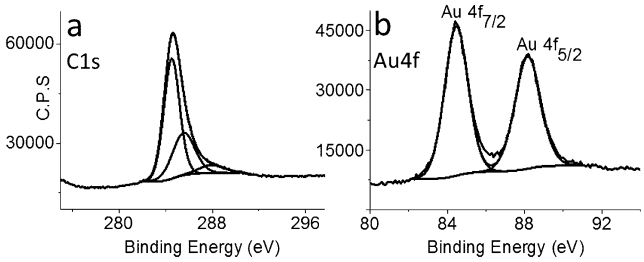

Figure 5. XPS C 1s (a) and Au 4f (b) peaks, as well as their best fitting to individual components recorded for the Au/fl-G sample (3.2 ng cm^{-2}).

(285.5 eV), and CO_2H (288.5 eV) C atoms, respectively. The Au 4f core level peak presents the expected two contributions owing to Au 4f5/2 and Au 4f7/2 separated by 3.73 eV, arising from spin-orbit splitting at 88.18 and 84.45 eV, respectively. The shape of the experimental Au 4f peak indicates that there is a single component, Au^0, without significant contribution of Au^I and Au^{III}. The binding energy values of the Au 4f peak in Au/fl-G are, however, shifted by 0.4 eV to higher values relative to bulk Au. This binding energy shift is again compatible with the occurrence of a strong gold–support interaction.

Supported Au NPs exhibit remarkable catalytic activity for a series of reactions, including selective oxidations, reductions, and couplings.[2,30,31] To evaluate the influence of preferential 1.1.1 facet orientation and the strong metal–support interaction on the catalytic performance, the activity of the Au/fl-G film (quartz plates, 3.2 ng cm^{-2}) was compared with that of an analogous Au/fl-G sample in which Au NPs obtained by the polyol method were deposited on fl-G at 0.1 wt % Au content. The polyol reduction is known to render Au NPs of about 5 nm average size.[32,33] The fl-G was obtained by pyrolysis of chitosan and subsequent exfoliation of the turbostratic carbon residue by sonication.[28] Preformed Au NPs were subsequently adsorbed on fl-G. Au/fl-G exhibited the XRD shown in Figure 1, devoid of any preferential facet orientation. The comparison of the influence of facet orientation and strong metal–support interaction was evaluated for two representative coupling reactions, namely, the Ullmann-like homocoupling of iodobenzene to biphenyl [Eq. (1), Table 1], the C–N cross coupling of anilines [Eq. (2)], and the degradative oxidation of benzene to benzoic acid [Eq. (3)].

Control experiments showed that fl-G does not exhibit any noticeable catalytic activity in comparison to that of the samples containing Au. In contrast, Au/fl-G films exhibited remarkable catalytic activity. Hot filtration tests removing the Au/fl-G plates after 8 h reaction time showed that the conversion stops in all cases. Furthermore, Au was not detected in the liquid phase after removal of Au/fl-G at final reaction time. When the catalytic activity of unoriented Au/fl-G sample was tested at the same Au/substrate mol ratio as Au/fl-G films (about 10^{-9}), no catalytic activity was observed. However, at higher Au/substrate mol ratio (about 10^{-3}), Au/fl-G was also significantly active. No leaching was observed for Au/fl-G powders. The results are collected in Table 1.

Table 1: Comparative activity data determined for **Au**/fl-G film and Au/fl-G.

Catalyst	Conversion [%]	Selectivity [%]	Turnover Number
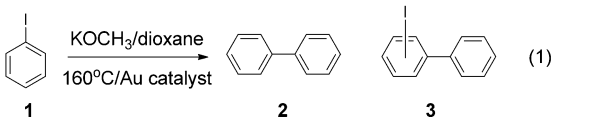			
		1	**2** **3** (1)
Au/fl-G film[a]	0.3	83 to **2** 16 to **3**	3.7×10^5
Au/fl-G[a,b]	0.2	100	79
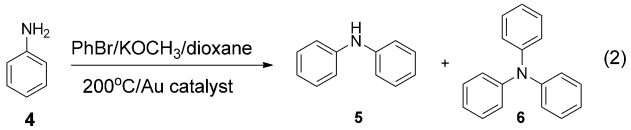			
		4	**5** **6** (2)
Au/fl-G film[c]	14.7	95.2 to **5** 4.8 to **6**	9.2×10^6
Au/fl-G[b,c]	5.1	100 to **5**	10
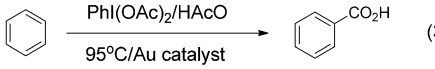			
		7	**8** (3)
Au/fl-G film[d]	23.9	100	1.4×10^7
Au/fl-G[b,d]	35.2	100	21.8

[a] Reaction conditions: Iodobenzene 2.00 mmol, 4 mL 1,4-dioxane, base = 2 mmol ($KOCH_3$), reaction temperature: 160 °C, time 24 h, catalyst: Au/fl-G films 1×1 cm^2 or Aufl-G powder 10 mg. [b] When exactly the same total amount of Au present in Au/fl-G is used for Au/fl-G, no reaction was observed (see text for comments). [c] Reaction conditions: Bromobenzene 1,2 mmol, aniline 1 mmol, $KOCH_3$ 2.1 mmol, 1,4-dioxane 4 mL, reaction temperature: 200 °C, time 24 h. [d] Reaction conditions: Benzene 10 mmol, $PhI(OAc)_2$ 1 mmol, solvent 17 mmol HOAc, reaction temperature: 95 °C, time = 24 h, catalyst: Au/fl-G films 1×1 cm^2 or Au/fl-G powder 10 mg.

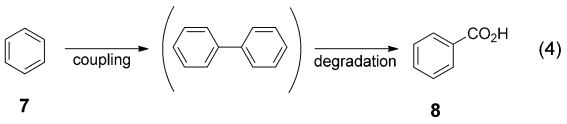

The Ullmann-like homocoupling of iodobenzene affords biphenyl as major product, accompanied by minor amounts of *ortho* and *para* isomers of iodobiphenyl. Similarly, the reaction of aniline and bromobenzene under basic conditions affords diphenylamine accompanied (Au/fl-G) or not (Au/fl-G) by triphenylamine, arising from the double C–N coupling. In the case of the oxidative degradation of benzene by phenyiodoso diacetate, biphenyl is the primary product that undergoes efficient degradation to form benzoic acid. As seen in [Eq. (4), Table 1] the carbon of the carboxylic acid group of benzoic acid derives from the oxidation of biphenyl intermediate. The most remarkable fact from Table 1 is that the turnover number values obtained for Au/fl-G film are all over six orders of magnitude higher than those of Au/fl-G for the same reaction. This higher catalytic activity is due to the high activity of minute amounts of Au when deposited as oriented nanoplatelets on fl-G, the preferential orientation of the Au nanoplatelets, and the occurrence of strong Au-G interactions, as evidenced by the particle size, the 2D band shift in

Raman, and the Au 4f binding energy in XPS. When a $\overline{Au}$/fl-G film with higher Au loading (2.4 $\mu g \times cm^{-2}$) was used as the catalyst, similar catalytic activities at the final reaction times were observed, but turnover numbers of these unoptimized loadings were about two orders of magnitude lower, probably owing to the larger Au nanocrystal size (up to 1000 nm). At the end of the reaction, the $\overline{Au}$/fl-G film becomes detached from the quartz plate, but could be recovered from the reaction mixture. A second use of the detached $\overline{Au}$/fl-G catalyst for the oxidative degradation showed similar catalytic activity (22%) as that of the fresh catalyst. Furthermore, SEM images of the used $\overline{Au}$/fl-G catalyst did not show significant changes in the morphology and size of the Au nanoplatelets (Figure S8).

In conclusion, we have shown a reliable procedure for the preparation of 1.1.1 facet-oriented Au nanoplatelets supported on fl-G by pyrolysis at 900 °C of a chitosan precursor containing $AuCl_4^-$. The resulting $\overline{Au}$/fl-G films exhibit an extremely high catalytic activity for coupling and oxidation reactions compared to unoriented Au/fl-G analogues. Although further work is necessary to fully clarify the origin of the remarkable catalytic activity, it seems that it derives from the combination of strong metal–support interaction and preferential facet orientation. Another issue is to show the general applicability of this procedure for other metals that do not dissolve on carbon, and assessment of any preferential facet orientation.

Experimental Section

Synthesis of few-layers graphene (fl-G): Alginic acid sodium salt from brown algae (Sigma) was pyrolyzed under argon atmosphere using the following oven program: annealing at 200 °C for 2 h, followed by heating at 10 °C min^{-1} up to 900 °C for 6 h. The resulting graphitic powder was sonicated at 700 W for 1 h in water and the residue removed by centrifugation to obtain fl-G dispersed in water.

Au NPs deposition on fl-G (0.1 % wt): fl-G from alginate pyrolysis (100 mg) was added to ethylene glycol (40 mL) and the mixture was sonicated at 700 W for 1 h to obtain dispersed fl-G. $HAuCl_4$ (0.2 mg) was added to the reaction mixture and Au metal reduction was then performed at 120 °C for 24 h with continuous stirring. The Au/fl-G were finally separated by filtration and washed exhaustively with water and acetone. The resulting material was dried in a vacuum desiccator at 110 °C to remove the remaining water. The amount of gold present on the films was determined by ICP-OES by immersing the plates into aqua regia (HNO_3/HCl 1:3) at room temperature for 3 h and analyzing the Au content of the resulting solution.

Synthesis of oriented Au NPs over few-layers graphene films ($\overline{\mathbf{Au}}$/fl-G): 0.5 g of chitosan from Aldrich (low molecular weight) was dissolved in water with a small quantity of acetic acid (0.23 g), which is necessary for complete dissolution of chitosan. The solution was filtered through a syringe of 0.45 μm diameter pore to remove impurities present in commercial chitosan. The films were supported on a quartz plate (2×2 cm^2) by casting 500 μL of filtered solution at 4000 rpm during 1 min. In the second synthesis step, the obtained chitosan films were immersed in a $HAuCl_4$ solution (1 mM or 0.01 mM) during 1 min. The pyrolysis was performed under argon atmosphere using the following oven program: heating rate at 5 °C min^{-1} up to 900 °C for 2 h. The amount of gold present on the films was determined by ICP-OES by immersing the plates into aqua regia at room temperature for 3 h and analyzing the Au content of the resulting solution.

General procedure for the Ullmann-like homocoupling: All reagents were purchased from Sigma–Aldrich and used as received without any purification. To a solution of iodobenzene (2.00 mmol) in 4 mL of 1,4-dioxane, $KOCH_3$ (2 mmol) and catalyst (1×1 cm^2 plate of $\overline{Au}$/fl-G film or 10 mg of Au/fl-G powder, 0.1 Au loading) were added. The resulting mixture was stirred in an autoclave for 24 h at 160 °C. After the reaction, the catalyst was collected by filtration and the reaction products were analyzed and identified by GC-MS (THERMO Electron Corporation instrument, Trace GC Ultra and DSQ, TraceGOLD): TG-5SilMS column with the following specifications: 30 m × 0.25 mm × 0.25 μm, working with a temperature program that starts at 50 °C maintained for 2 min and afterwards increasing the temperature at a rate of 10 °C min^{-1} up to 250 °C that was maintained for 10 min, resulting in a total run time of 32 min. The pressure of He used as the carrier gas was 0.38 Torr. Mass spectra of the products were acquired at 70000 resolutions. Biphenyl (**2**): MS (EI) *m*/*z* (rel.int): 154 (M^+, 100%), 128 (4), 115 (4), 76 (12), 63 (3), 51 (3); *o*-Iododiphenyl (**3a**): MS (EI) *m*/*z* 23(rel.int): 280 (M^+, 66.8%), 152 (100), 140 (8), 127 (8), 76 (14), 63 (4); *p*-iododiphenyl (**3b**): MS (EI) *m*/*z* (rel. int): 280 (M^+, 100%), 152(78), 140 (6), 127 (7), 76 (12), 63 (3).

General procedure for the C-N reaction: To a solution of bromobenzene (1.2 mmol) and aniline (1 mmol) in 4 mL of 1,4-dioxane, $KOCH_3$ (2.1 mmol) and catalyst were added. The resulting mixture was stirred in an autoclave for 24 h at 200 °C. After the reaction, the catalyst was collected by filtration and the reaction products were analyzed and identified by GC-MS (THERMO Electron Corporation instrument).

Diphenylamine (**5**): MS (EI) *m*/*z* (rel.int): 169 (M^+, 100%), 141 (5), 115 (4), 84 (12), 77 (5), 51 (3); Triphenylamine (**6**): MS (EI) *m*/*z* (rel.int): 245 (M^+, 100%), 167 (22), 141 (12), 115 (9), 77 (10), 51 (5).

General procedure for the oxidative coupling reaction: To a solution of benzene (10 mmol) and 1 mmol of oxidant [$PhI(OAc)_2$], acetic acid (17 mmol) and catalyst were added. The mixture was stirred for 24 h at 95 °C in an autoclave, and then quenched with water (10 mL). The reaction mixture was extracted with EtOAc (3×10 mL) and the combined organic layer was washed with saturated $NaHCO_3$ (2×20 mL), brine (10 mL), dried over Na_2SO_4, filtered, and concentrated. The products were analyzed and identified by using GC-MS (THERMO Electron Corporation instrument) and a Bruker Advance III UltraShield 500 MHz spectrometer, operating at 500.13 MHz for ^1H NMR, 125.77 MHz for ^{13}C NMR. Turnover numbers were calculated by dividing the moles of product formed by the moles of Au present in the catalyst at final reaction time.

Acknowledgements

Financial support by the Spanish Ministry of Economy and Competitiveness (Severo Ochoa and CTQ2012-32315) and by the Generalidad Valenciana (Promoteo 2013-019) is gratefully acknowledged. I.E-A. thanks the Spanish Ministry for a postgraduate scholarship. SMC, NC, and VIP thank PNCDI II, project 275/2011, for the financial support. We are thankful to Mrs. Amparo Forneli for her assistance in sample preparation.

Keywords: coupling catalysts · graphene support · heterogeneous catalysis · oriented gold nanoparticles

How to cite: *Angew. Chem. Int. Ed.* **2016**, *55*, 607–612
Angew. Chem. **2016**, *128*, 617–622

[1] D. Astruc, F. Lu, J. R. Aranzaes, *Angew. Chem. Int. Ed.* **2005**, *44*, 7852–7872; *Angew. Chem.* **2005**, *117*, 8062–8083.

[2] A. S. K. Hashmi, G. J. Hutchings, *Angew. Chem. Int. Ed.* **2006**, *45*, 7896 – 7936; *Angew. Chem.* **2006**, *118*, 8064 – 8105.
[3] A. S. K. Hashmi, *Angew. Chem. Int. Ed.* **2005**, *44*, 6990 – 6993; *Angew. Chem.* **2005**, *117*, 7150 – 7154.
[4] M. Haruta, S. Tsubota, T. Kobayashi, H. Kageyama, M. J. Genet, B. Delmon, *J. Catal.* **1993**, *144*, 175 – 192.
[5] M. Boronat, D. Combita, P. Concepción, A. Corma, H. García, R. Juárez, S. Laursen, J. de Dios López-Castro, *J. Phys. Chem. C* **2012**, *116*, 24855 – 24867.
[6] J. Lin, H. Abroshan, C. Liu, M. Zhu, G. Li, M. Haruta, *J. Catal.* **2015**, *330*, 354 – 361.
[7] V. K. Kanuru, G. Kyriakou, S. K. Beaumont, A. C. Papageorgiou, D. J. Watson, R. M. Lambert, *J. Am. Chem. Soc.* **2010**, *132*, 8081 – 8086.
[8] Q. Zhang, H. Wang, *ACS Catal.* **2014**, *4*, 4027 – 4033.
[9] G. Li, C. Zeng, R. Jin, *J. Phys. Chem. C* **2015**, *119*, 11143 – 11147.
[10] B. Goris, S. Bals, W. Van den Broek, E. Carbó-Argibay, S. Gómez-Granza, L. M. Liz-Marzán, G. Van Tendeloo, *Nat. Mater.* **2012**, *11*, 930 – 935.
[11] A. R. Tao, S. Habas, P. Yang, *Small* **2008**, *4*, 310 – 325.
[12] P. Prodhomme, S. Warren, R. Cortes, H. F. Jurca, F. Maroun, P. Allongue, *ChemPhysChem* **2010**, *11*, 2992 – 3001.
[13] Y. G. Sun, Y. N. Xia, *Science* **2002**, *298*, 2176 – 2179.
[14] C.-C. Chen, C.-H. Hsu, P.-L. Kuo, *Langmuir* **2007**, *23*, 6801 – 6806.
[15] C. J. Johnson, E. Dujardin, S. A. Davis, C. J. Murphy, S. Mann, *J. Mater. Chem.* **2002**, *12*, 1765 – 1770.
[16] X. Chen, G. Wu, J. Chen, X. Chen, Z. Xie, X. Wang, *J. Am. Chem. Soc.* **2011**, *133*, 3693 – 3695.
[17] S. Guo, S. Sun, *J. Am. Chem. Soc.* **2012**, *134*, 2492 – 2495.
[18] J. Albero, H. Garcia, *J. Mol. Catal. A* **2015**, *408*, 296 – 309.
[19] A. Primo, I. Esteve-Adell, J. F. Blandez, D. A., M. Alvaro, N. Candu, S. N. Coman, V. I. Parvulescu, H. Garcia, *Nat. Commun.* **2015**, DOI: 2015/ncomms11406a.
[20] A. Primo, P. Atienzar, E. Sanchez, J. M. Delgado, H. Garcia, *Chem. Commun.* **2012**, *48*, 9254 – 9256.
[21] X. Li, W. Cai, J. An, S. Kim, J. Nah, D. Yang, R. Piner, A. Velamakanni, I. Jung, E. Tutuc, S. K. Banerjee, L. Colombo, R. S. Ruoff, *Science* **2009**, *324*, 1312 – 1314.
[22] D. Takagi, Y. Kobayashi, H. Hlbirio, S. Suzuki, Y. Homma, *Nano Lett.* **2008**, *8*, 832 – 835.
[23] G. Goncalves, P. A. A. P. Marques, C. M. Granadeiro, H. I. S. Nogueira, M. K. Singh, J. Grãcio, *Chem. Mater.* **2009**, *21*, 4796 – 4802.
[24] M. Quintana, K. Spyrou, M. Grzelczak, W. R. Browne, P. Rudolf, M. Prato, *ACS Nano* **2010**, *4*, 3527 – 3533.
[25] W. Liu, H. Li, C. Xu, Y. Khatami, K. Banerjee, *Carbon* **2011**, *49*, 4122 – 4130.
[26] C. Mattevi, H. Kima, M. Chhowalla, *J. Mater. Chem.* **2010**, *20*, 3324 – 3334.
[27] P. W. Trimby, *Ultramicroscopy* **2012**, *120*, 16 – 24.
[28] A. Primo, E. Sánchez, J. M. Delgado, H. García, *Carbon* **2014**, *68*, 777 – 783.
[29] A. C. Ferrari, D. M. Basko, *Nat. Nanotechnol.* **2013**, *8*, 235 – 246.
[30] M. Stratakis, H. Garcia, *Chem. Rev.* **2012**, *112*, 4469 – 4506.
[31] A. S. K. Hashmi, *Chem. Rev.* **2007**, *107*, 3180 – 3211.
[32] C. Luo, Y. Zhang, X. Zeng, Y. Zeng, Y. Wang, *J. Colloid Interface Sci.* **2005**, *288*, 444 – 448.
[33] B. K. Park, S. Jeong, D. Kim, J. Moon, S. Lim, J. S. Kim, *J. Colloid Interface Sci.* **2007**, *311*, 417 – 424.

Received: September 23, 2015
Revised: October 26, 2015
Published online: November 24, 2015

